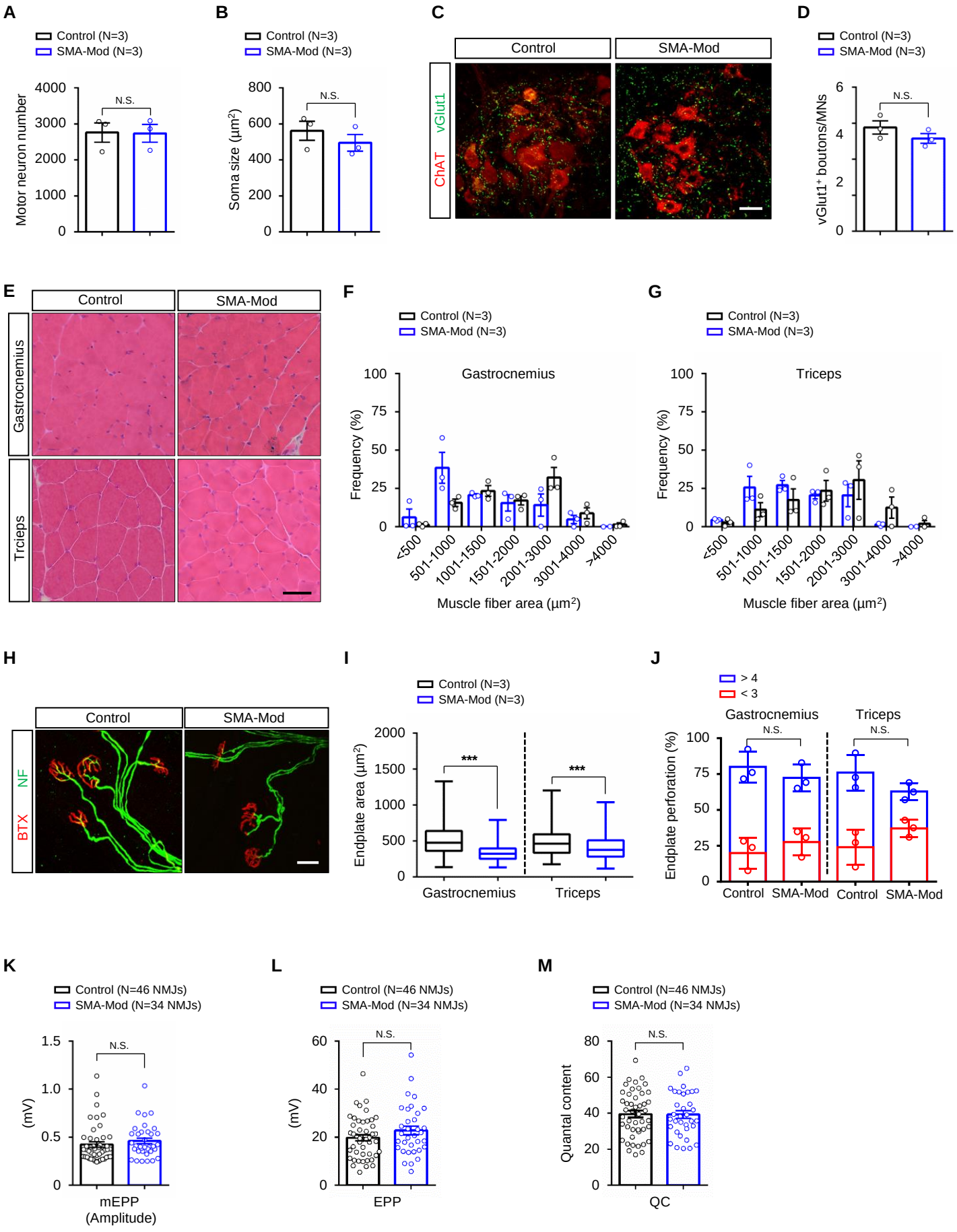
A
Control (N=3)
SMA-Mod (N=3)
Motor neuron number
4000
3000
2000
1000
0
N.S.
B
Control (N=3)
SMA-Mod (N=3)
Soma size (μm²)
800
600
400
200
0
N.S.
C
Control
SMA-Mod
ChAT
vGlut1
D
Control (N=3)
SMA-Mod (N=3)
vGlut1⁺ boutons/MNs
6
4
2
0
N.S.
E
Control
SMA-Mod
Gastrocnemius
Trcieps
F
Control (N=3)
SMA-Mod (N=3)
Gastrocnemius
Frequency (%)
100
75
50
25
0
<500
501-1000
1001-1500
1501-2000
2001-3000
3001-4000
>4000
Muscle fiber area (μm²)
G
Control (N=3)
SMA-Mod (N=3)
Triceps
Frequency (%)
100
75
50
25
0
<500
501-1000
1001-1500
1501-2000
2001-3000
3001-4000
>4000
Muscle fiber area (μm²)
H
Control
SMA-Mod
BTX
NF
I
Control (N=3)
SMA-Mod (N=3)
Endplate area (μm²)
2000
1500
1000
500
0
***
***
Gastrocnemius
Triceps
J
> 4
< 3
Gastrocnemius
Triceps
N.S.
N.S.
Endplate perforation (%)
100
75
50
25
0
Control
SMA-Mod
Control
SMA-Mod
K
Control (N=46 NMJs)
SMA-Mod (N=34 NMJs)
(mV)
1.5
1.0
0.5
0
N.S.
mEPP
(Amplitude)
L
Control (N=46 NMJs)
SMA-Mod (N=34 NMJs)
(mV)
60
40
20
0
N.S.
EPP
M
Control (N=46 NMJs)
SMA-Mod (N=34 NMJs)
Quantal content
80
60
40
20
0
N.S.
QC

Figure S1

Figure S1. Mitigation of neuromuscular pathology in mixed-strain modified SMA-Mod mutants; related to Figure 1. Thoracic motor neurons in modified SMA mutants are (A), neither reduced in numbers nor (B), altered in size at PND70. (C) Representative transverse sections of thoracic spinal cord depicting equivalent numbers of vGlut1-positive proprioceptive sensory afferents on motor neuron soma of an adult (PND70) SMA modified and control mouse. (D) Quantified results of vGlut1 boutons on motor neurons of SMA-Mod and littermate controls. (E) Hematoxylin-eosin (H&E) stained transverse sections of indicated muscles from modified SMA mice and controls show morphologically normal fibers in the former. Frequency distributions of fiber areas in (F) the gastrocnemius and (G) the triceps are illustrative of smaller fibers in the modified mutants. (H) Representative NMJs in young adult modified mutants and controls. Mutant NMJs were found to be (I) smaller but (J) fully mature and functionally equivalent to control endplates as assessed by (K) mEPP amplitudes, (L) EPPs and (M) quantal content. Note: ***, $P < 0.001$, *t* tests; N.S. – not significant. Scale bars: 35μm, 35μm, 25μm respectively for panels (C, E and H). Controls – SMA carrier mice heterozygous for murine *Smn*. Data: mean ± SEM.

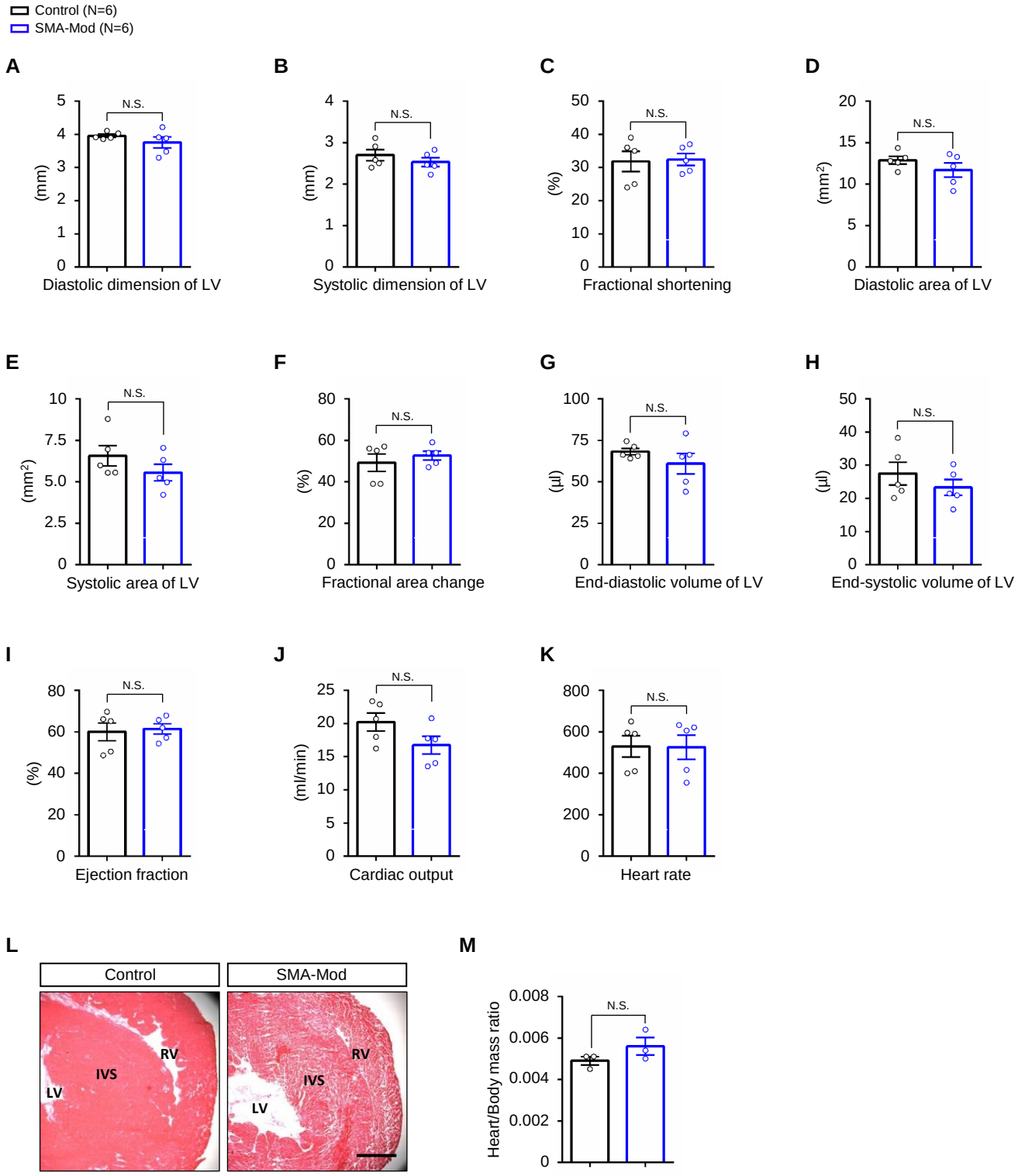

Figure S2. Cardiac function is preserved in SMA-Mod mutants; related to Figure 1. Echocardiography was employed to quantify results of (A) diastolic and (B) systolic left ventricular dimensions in young adult controls and modified SMA mutants; no change in these measures were detected in mutants. (C) Fractional shortening, (D) diastolic and (E) systolic left ventricular areas, (F) fractional area change, (G) end-diastolic and (H) end systolic left ventricular volumes, (I) ejection fractions, (J) cardiac output and (K) heart rate were similarly found to be preserved in modified mutants. (L) H&E stains of transverse sections through the hearts of modified SMA mutants and controls depict morphologically normal cardiac structure in the latter as assessed by the thickness of the left ventricular wall. LV – left ventricle, RV – right ventricle, IVS – intra-ventricular space. (M) Quantified results of heart to body mass ratios signify normal heart size in the mutants. Note: N.S. – not significant, *t* tests. Scale bar: 600µm. Data: mean ± SEM.

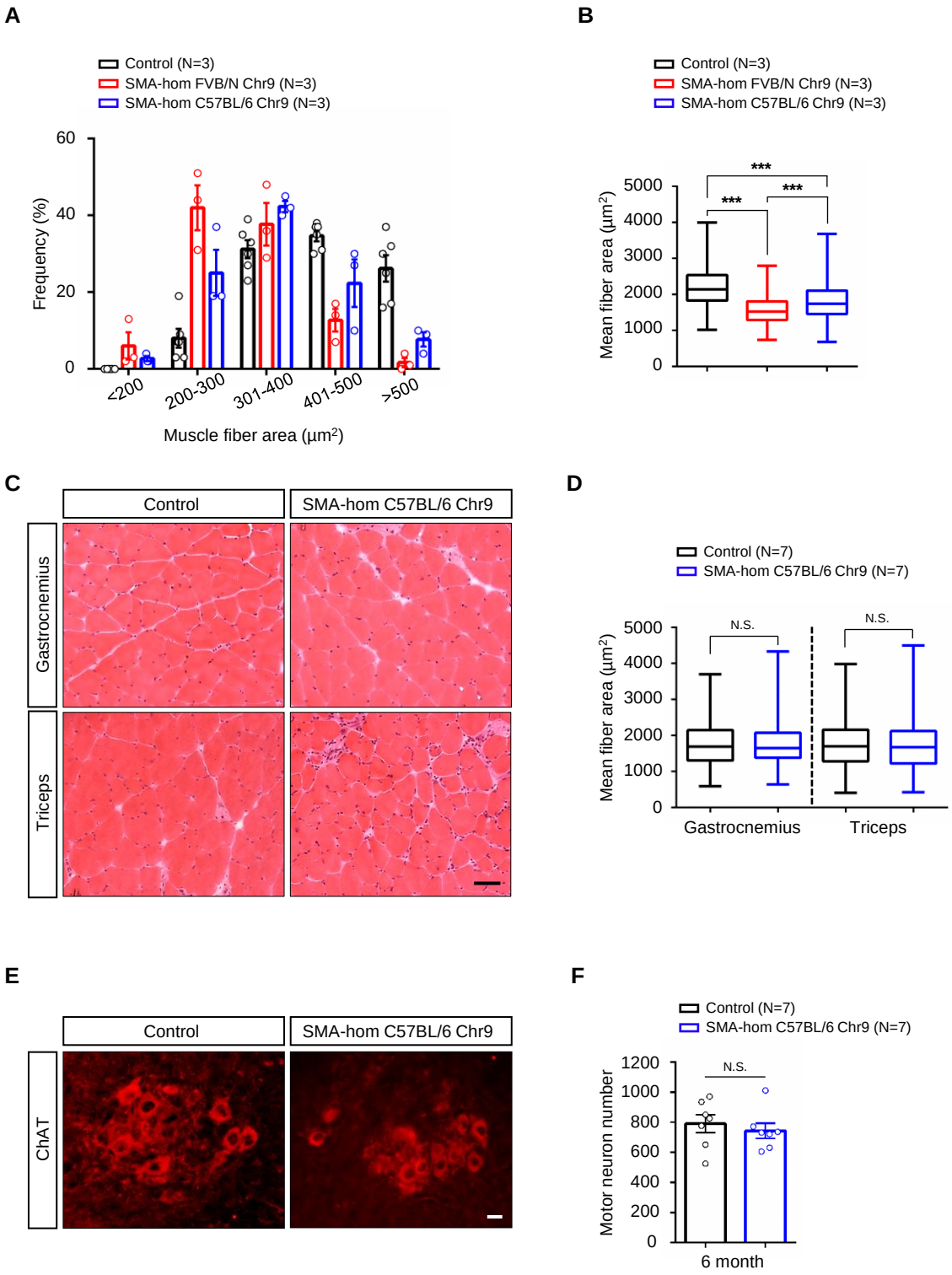

Figure S3. Rescue of muscle and motor neuron defects in modified FVB/N mutants harboring the Chr.9 ROI; related to Figure 1. (A) Frequency distribution analysis and (B) quantified results of mean gastrocnemius myofiber area in PND7 mice are illustrative of reduced muscle atrophy in modified mutants. ***, $P < 0.001$, one-way ANOVA. (C) H&E-stained muscle sections from a 6-month-old mutant and littermate control showing similar myofiber morphology in the two. (D) Quantified results of fiber areas in the two cohorts of mice. (E) Representative immunostains of spinal cord sections depicting equivalent numbers and morphologically normal ventral horn motor neurons in a 6-month-old modified mutant. (F) Quantified results of lumbar motor neurons in mutants and littermate controls. Note: N.S. – not significant, *t* tests for panels (D and F). Scale bars: 35μm, panel (C); 20μm, panel (E). Data: mean ± SEM.

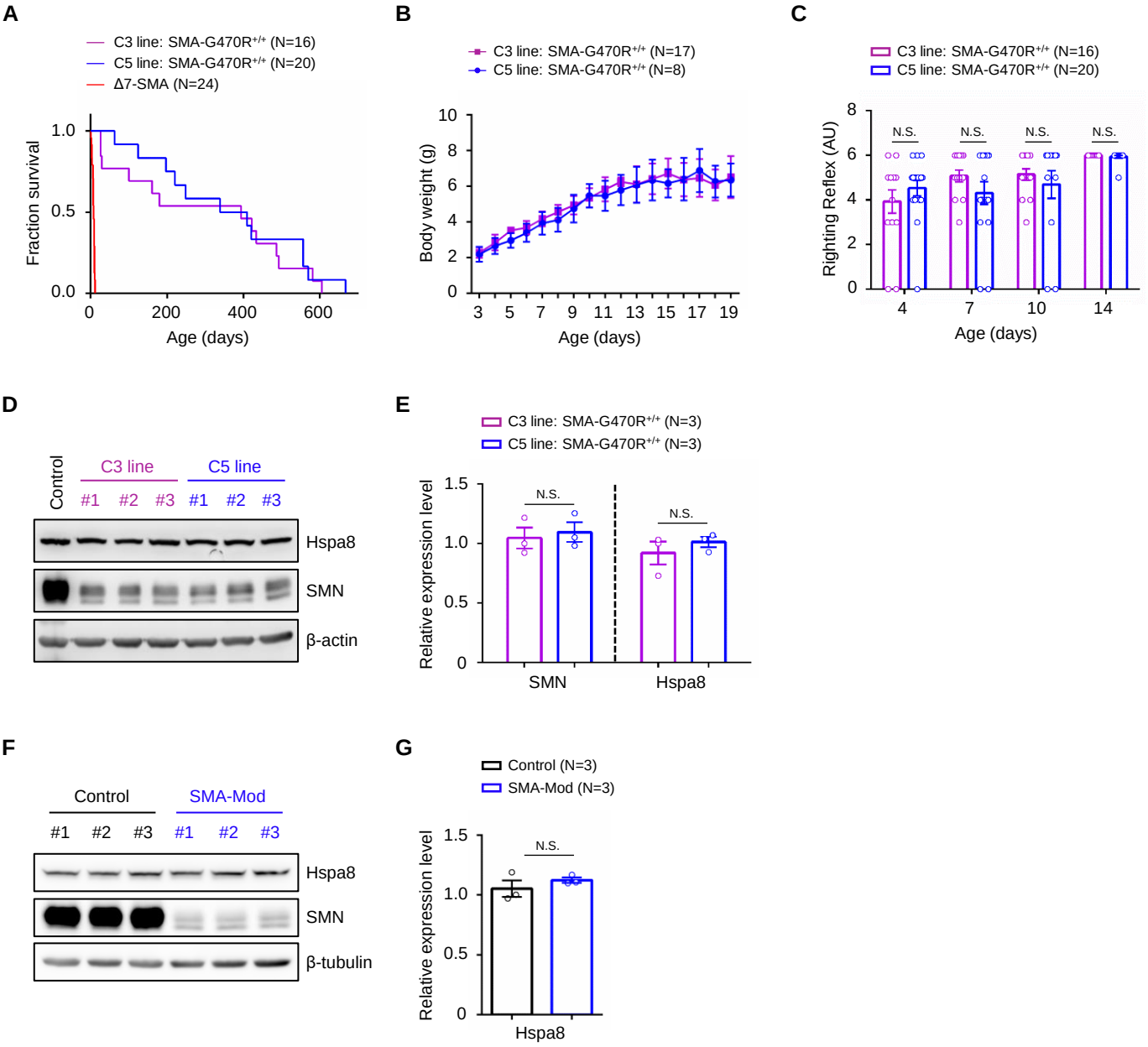

Figure S4. The SMA phenotype is similarly modified in independent lines expressing the Hspa8^{G470R} variant; related to Figure 3. (A) Kaplan-Meier survival curves depicting a profound extension of lifespan in each of two independent SMA mutant lines gene edited to express the G470R variant. $P < 0.001$ between Δ7 SMA mutants and SMA-G470R$^{+/+}$ mutants from each of the C3 and C5 lines, $P = 0.5694$ between mutants from the C3 and C5 lines, log-rank test. (B) Body weight curves and (C) motor performance of mutants from the two lines suggesting equivalence between the lines. (D) Western blot of spinal cord tissue depicts identical levels of Hspa8 and SMN in 5-week-old mutants from the C3 and C5 lines. (E) Quantified results of blot in panel D. (F) Western blot demonstrates that the G470R alteration does not alter Hspa8 protein stability in SMA mutants. (G) Quantified results of Hspa8 protein in the blot in panel F. Note: N.S. – not significant, *t* tests in all relevant panels. Data: mean ± SEM.

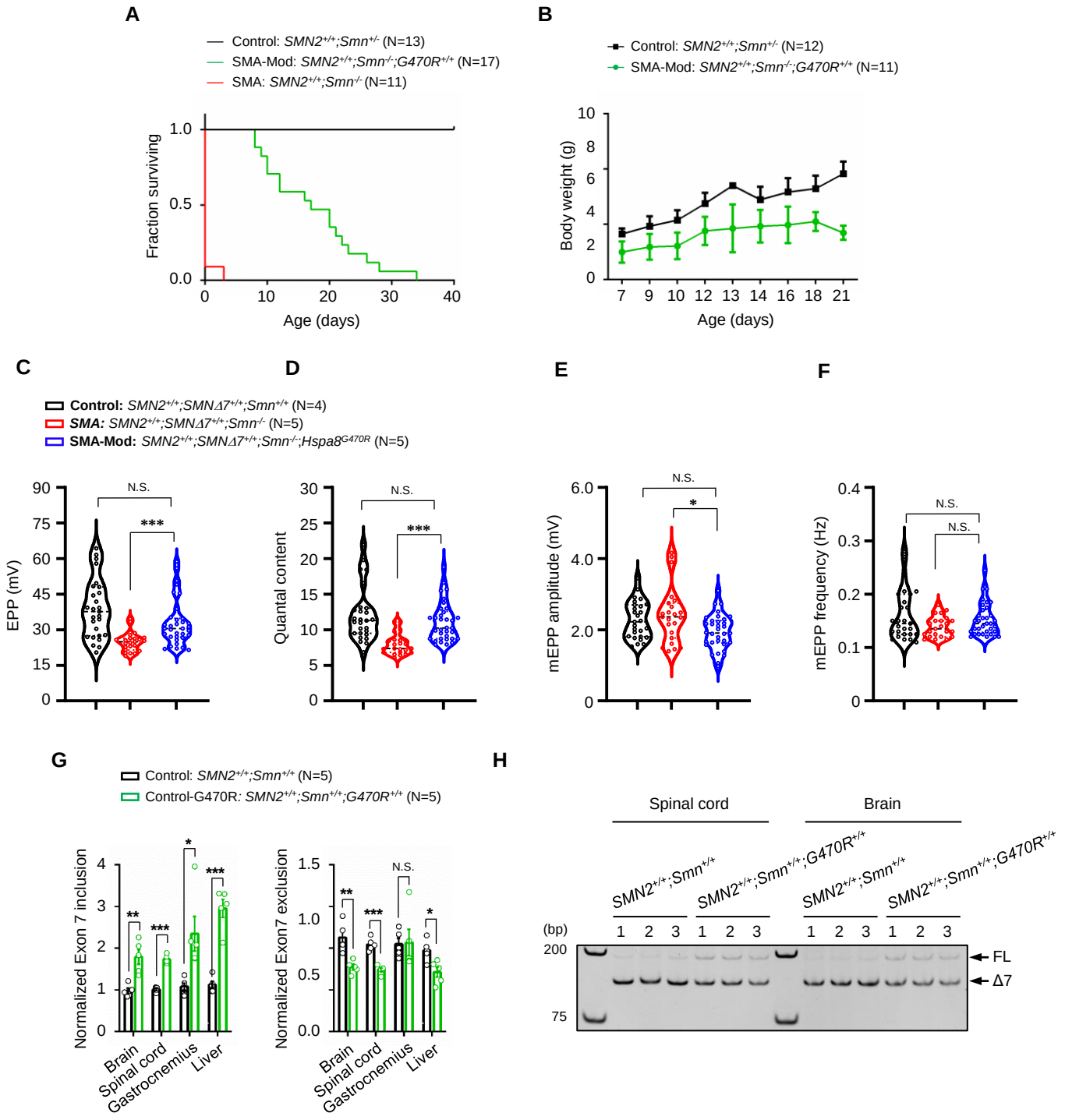

Figure S5. The Hspa8^{G470R} variant modifies disease in a second line of SMA mice and restores NMJ function in SMNΔ7 mutants; related to Figures 4, 5. (A) Hspa8^{G47R} expression enhances lifespans of very severely affected SMA mice on the FVB/N strain background. $P < 0.001$ between the two sets of mutants, log-rank test. (B) Graphs of growth trajectories in controls and mutant littermates homozygous for the G470R variant. Note: Mutants WT for Hspa8 failed to survive, precluding similar comparisons during the period of study. Neurotransmission, in young postnatal SMNΔ7 SMA mutants harboring the Hspa8^{G470R} variant, is normalized based on electro-physiological recordings in the transverse abdominus muscle measuring (C) Evoked potentials, and (D) quantal content. (E) MEPP amplitudes and (F) MEPP frequencies were also recorded in the same cohorts of mice. (G) Quantified results of real-time PCR experiments to ascertain relative FL-SMN and SMNΔ7 transcript levels in tissues of PND9 *SMN2*-expressing mice harboring either the WT or G470R variant of Hspa8. (H) Polyacrylamide gel analysis of the two transcripts from brain and spinal cord tissue of the two cohort of mice illustrates the splice-switching effect of Hspa8^{G470R}. Note: *, **, ***, $P < 0.05$, $P < 0.01$, $P < 0.001$ respectively, Kruskal-Wallis test for panels C, D & F, one-way ANOVA for panel E, *t* tests for panel G. N.S. – not significant. Data: mean ± SEM.

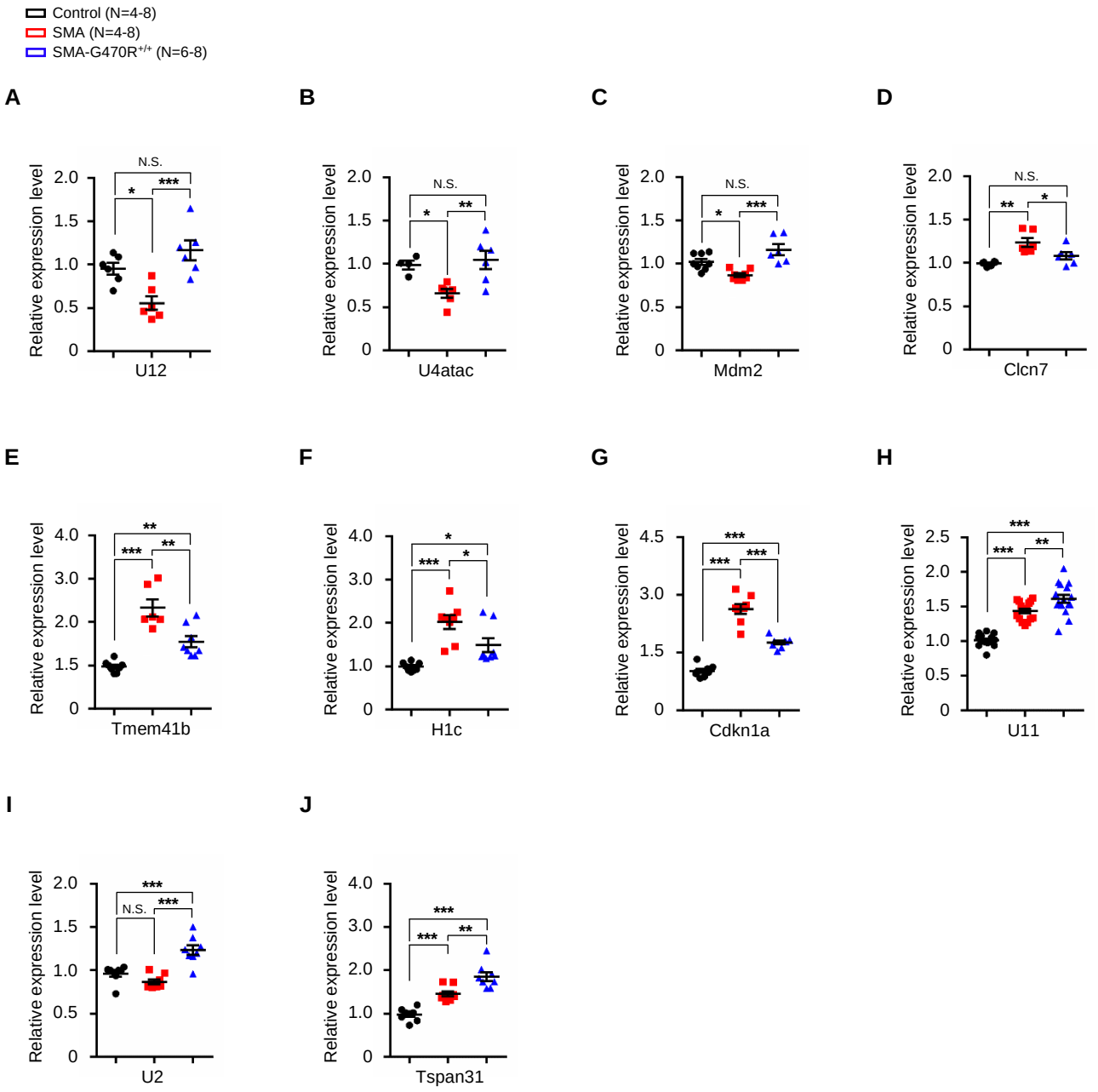

Figure S6. Incomplete rescue of mis-spliced or altered SMN target transcripts in SMA-G470R mutants; related to Figure 5. Relative RNA levels of (A) *U12* and (B) *U4atac* snRNAs in spinal cord tissue of PND9 controls and SMA mutants with or without the G470R variant. Levels of mis-spliced (C) *Mdm2* and (D) *Clcn7* transcripts were similarly quantified and were normalized in SMA-G470R mutants. In contrast, (E) mis-spliced *Tmem41b*, (F) improperly processed *H1c*, and (G) abnormal *Cdkn1a* transcript levels persisted. Graphs depicting (H) an exacerbation of altered *U11* snRNA levels in SMA-G470R mutants, (I) perturbed *U2* snRNA concentrations and (J) a dramatic increase in mis-spliced *Tspan31* in the mice. Note: *, **, ***, $P < 0.05$, $P < 0.01$, $P < 0.001$ respectively, one-way ANOVA. N.S. – not significant. Data: mean ± SEM.

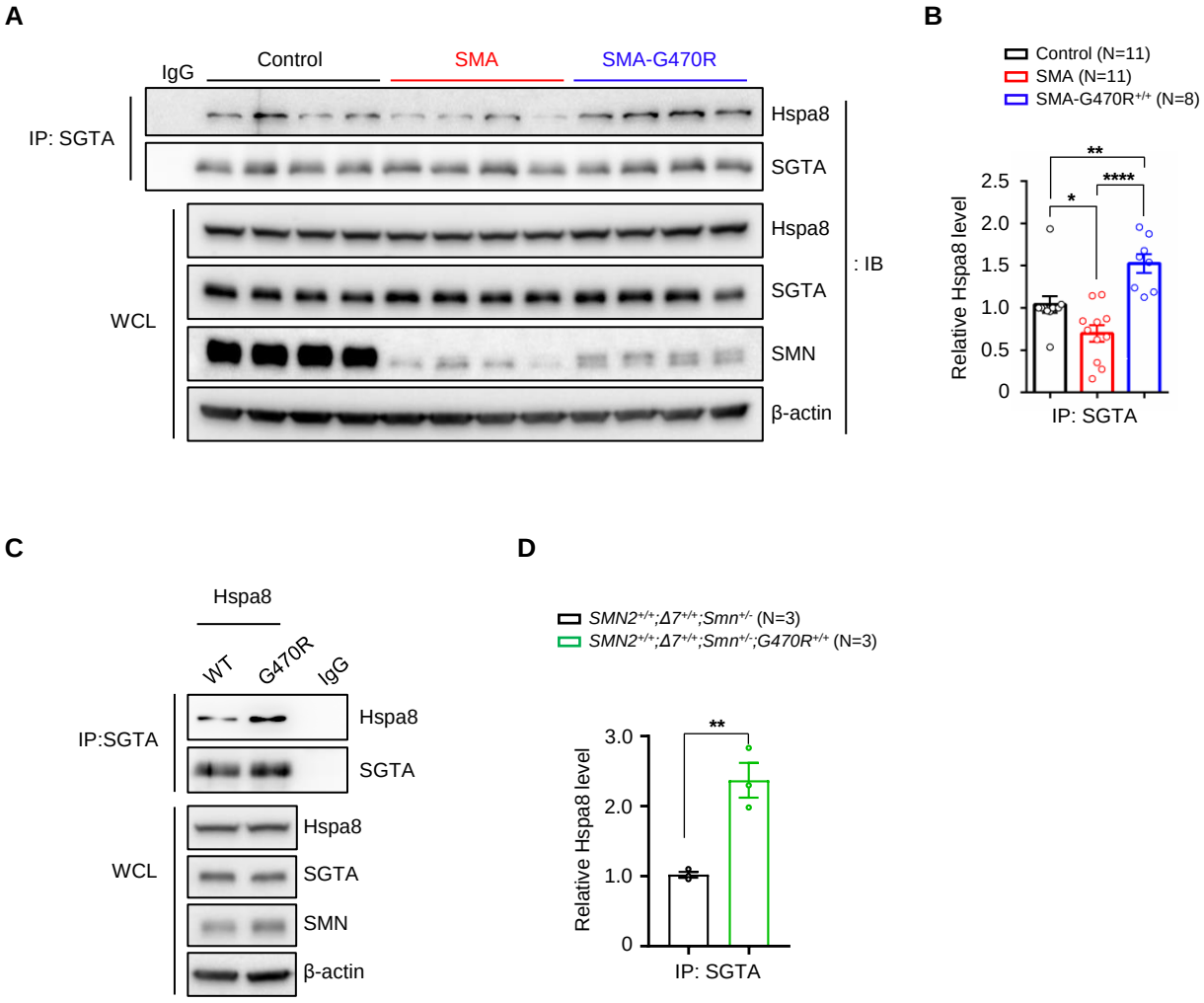

Figure S7. Enhanced avidity of Hspa8^{G470R} with co-chaperones is independent of its effects on SMN; related to Figure 6. (A) Co-IP analysis of brain-derived Hspa8^{WT} or Hspa8^{G470R} in PND9 controls and SMA mutants. (B) Quantified results of co-IP study. Note: *, **, ***, $P < 0.05$, $P < 0.01$, $P < 0.001$ respectively, one-way ANOVA. (C) Co-IP of Hspa8 and SGTA in controls with or without the G470R variant. (D) Quantified results of co-IP analysis in panel C. **, $P < 0.01$, *t* test. Data: mean ± SEM.

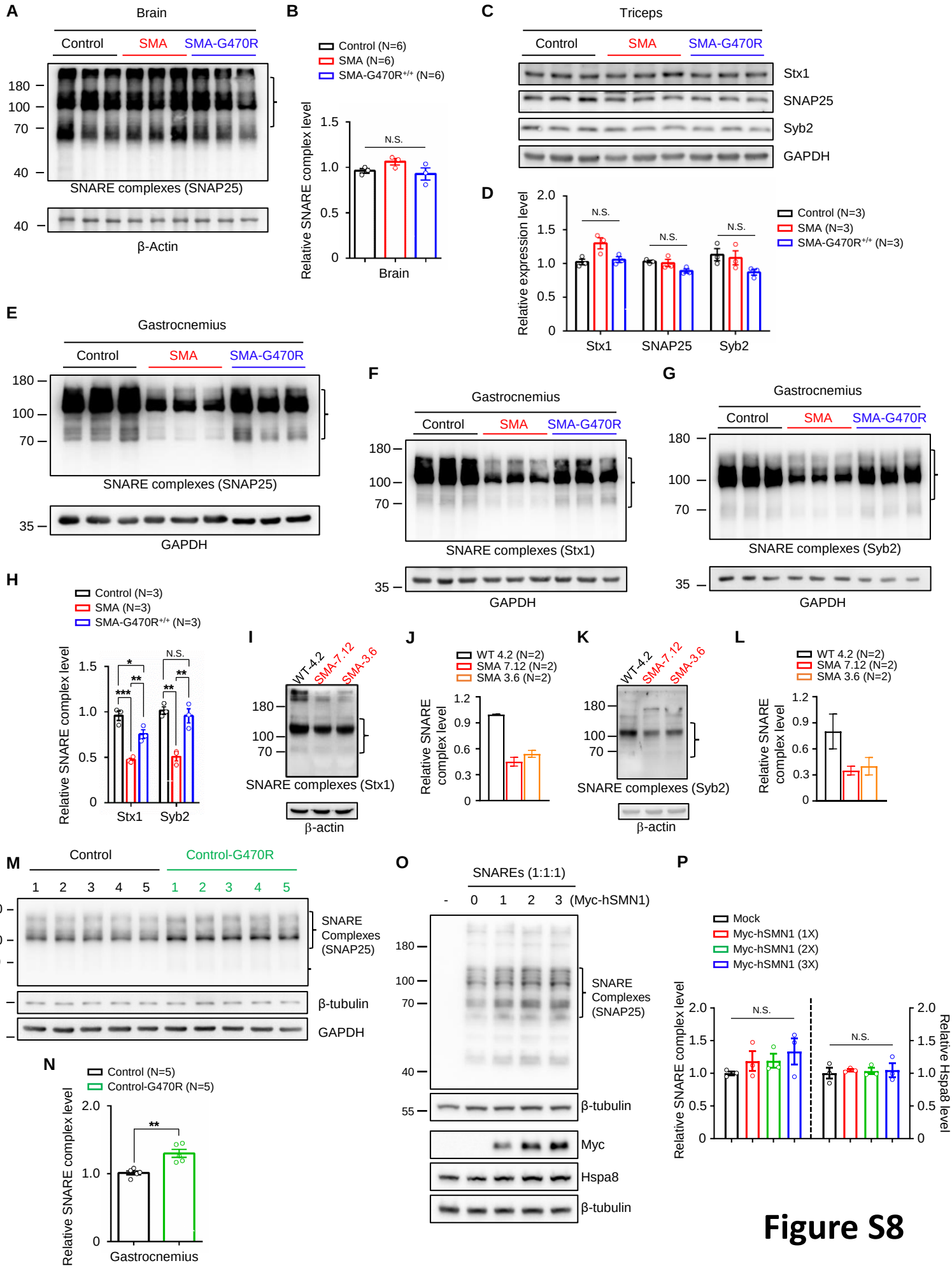
A
Brain
Control
SMA
SMA-G470R
180
100
70
40
SNARE complexes (SNAP25)
40
β-Actin
B
Control (N=6)
SMA (N=6)
SMA-G470R+/+ (N=6)
Relative SNARE complex level
N.S.
Brain
C
Triceps
Stx1
SNAP25
Syb2
GAPDH
D
Relative expression level
N.S.
Control (N=3)
SMA (N=3)
SMA-G470R+/+ (N=3)
Stx1
SNAP25
Syb2
E
Gastrocnemius
SNARE complexes (SNAP25)
35
GAPDH
F
Gastrocnemius
SNARE complexes (Stx1)
GAPDH
G
Gastrocnemius
SNARE complexes (Syb2)
GAPDH
H
Control (N=3)
SMA (N=3)
SMA-G470R+/+ (N=3)
Relative SNARE complex level
N.S.
Stx1
Syb2
I
WT-4.2
SMA-7.12
SMA-3.6
SNARE complexes (Stx1)
β-actin
J
WT 4.2 (N=2)
SMA 7.12 (N=2)
SMA 3.6 (N=2)
Relative SNARE complex level
K
WT-4.2
SMA-7.12
SMA-3.6
SNARE complexes (Syb2)
β-actin
L
WT 4.2 (N=2)
SMA 7.12 (N=2)
SMA 3.6 (N=2)
Relative SNARE complex level
M
Control
Control-G470R
1 2 3 4 5 1 2 3 4 5
SNARE Complexes (SNAP25)
β-tubulin
GAPDH
N
Control (N=5)
Control-G470R (N=5)
Relative SNARE complex level
Gastrocnemius
O
SNAREs (1:1:1)
- 0 1 2 3 (Myc-hSMN1)
SNARE Complexes (SNAP25)
β-tubulin
Myc
Hspa8
β-tubulin
P
Mock
Myc-hSMN1 (1X)
Myc-hSMN1 (2X)
Myc-hSMN1 (3X)
Relative SNARE complex level
N.S.
Relative Hspa8 level

Figure S8

Figure S8. Hspa8^{G470R} expression mitigates poor SNARE complex assembly in SMA; related to Figure 7. (A) Immunoblot depicting relatively normal SNARE complex levels in (curly bracket) brain tissue of PND9 SMA mice; samples were not boiled. (B) Quantified SNARE complex levels in samples analyzed for study depicted in panel (A). N.S. – not significant, one-way ANOVA. (C) Western blot of boiled lysates from the indicated cohorts of mice illustrates equivalent levels of uncomplexed (monomeric) SNAP25, Stx1 and Syb2 SNARE proteins in SMA and control animals. (D) Quantified results of blot in panel (C). N.S. – not significant, one-way ANOVA. (E) Blot shows reduced SNARE complexes in PND9 SMA NMJs derived from gastrocnemius muscle; complex levels are restored in SMA-G470R mutants. Similar patterns were observed when SNARE complexes were detected with antibodies against (F) Syntaxin1 and (G) Synaptobrevin2. (H) Graph showing relative SNARE complex levels quantified in the previous two panels. Note: *, **, ***, $P < 0.05$, $P < 0.01$, $P < 0.001$ respectively, one-way ANOVA. N.S. – not significant. (I) Immunoblot of SNARE complexes in hiPSC-derived motor neurons detected by an antibody to Stx1 and (J) Quantification of complex levels in such blots. (K) Blot of SNARE complexes in hiPSC-derived motor neurons detected by an antibody against Syb2 and (L) Quantification of complex levels in such blots. (M) Immunoblot shows more efficient SNARE complex assembly in gastrocnemius-derived NMJs from controls harboring the G470R variant. (N) Quantified results of SNARE complex levels in panel (M). Note: *, $P < 0.05$ *t* test. (O) Immunoblot of un-boiled samples from HEK293 cells transfected with the core SNARE components depicting unchanged SNARE complex formation under supra-physiologic SMN levels. The three lower blots in the panel depict loading controls from boiled lysates and demonstrate relatively stable levels of Hspa8 but increasing concentrations of Myc-SMN, as detected with anti-myc antibody. (P) Quantified levels of SNARE complexes and Hspa8 respectively in panel (O). Note: N.S. – not significant, one-way ANOVA. Data: mean ± SEM.

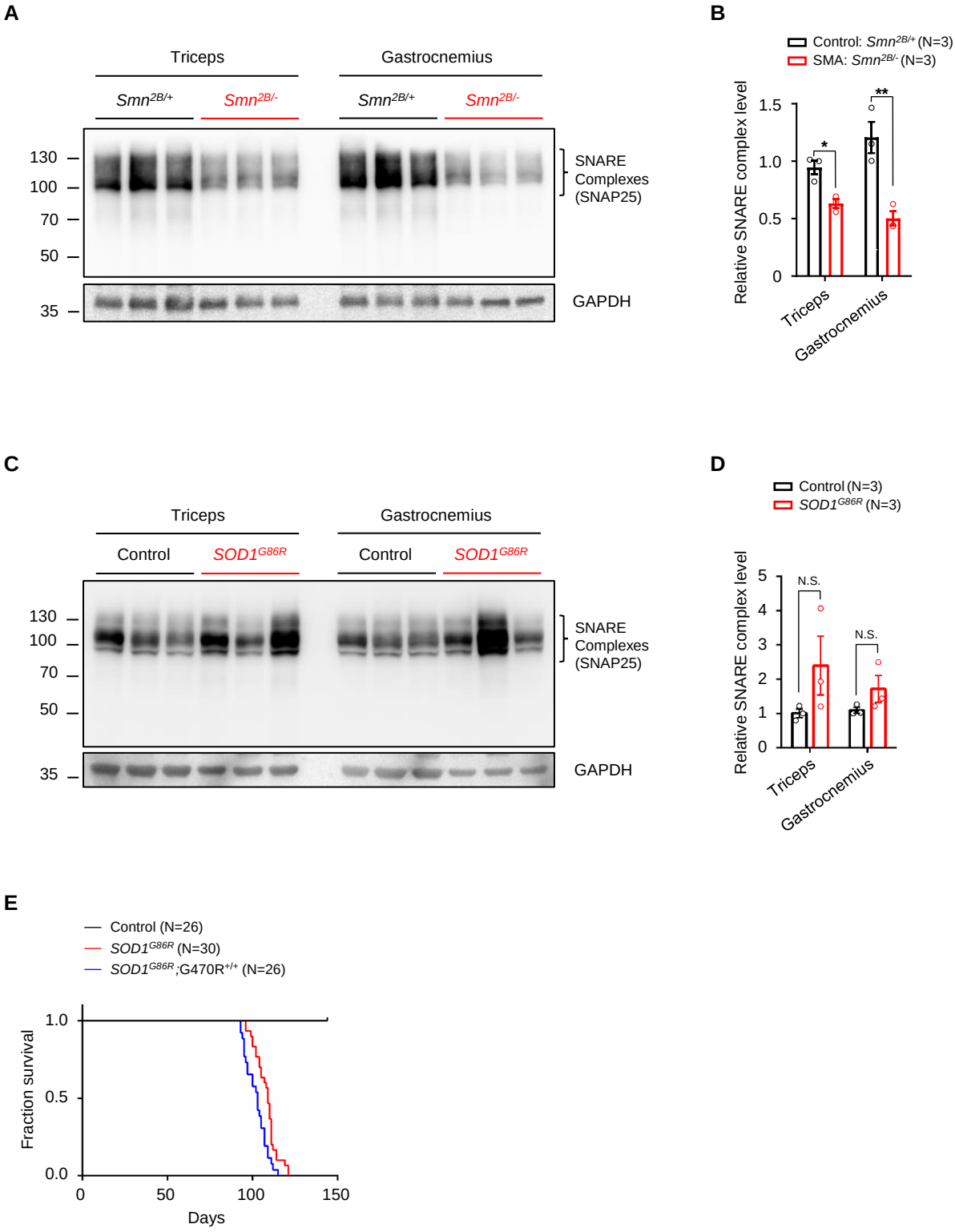

Figure S9. Poor SNARE complex assembly characterizes a second SMA line but is not a general feature of denervation; related to Figure 7. (A) Representative immunoblot depicting reduced high molecular weight SDS-resistant SNARE complexes in PND15 SMA NMJs derived from triceps and gastrocnemius muscles of $Smn^{2B/-}$ mutants; samples were not boiled. (B) Quantified results of SNARE complexes from previous panel. *, $P < 0.05$, *t* tests. (C) Blot shows unchanged SNARE complex levels in muscle NMJs of a symptomatic mouse model of ALS; samples were not boiled. (D) Quantified results of SNARE complexes from previous panel. N.S. – not significant, *t* tests. (E) Kaplan-Meier survival curves show that $Hspa8^{G470R}$ does not confer protection against the ALS phenotype in model mice. $P > 0.05$ between the two sets of SOD1 mutants, log-rank test. Data: mean ± SEM.